Physica Scripta

PAPER

Feynman's method in chiral nanorod-based metamaterial nanoplasmonics

Andrei Galiautdinov

Department of Physics and Astronomy, University of Georgia, Athens, GA 30602, United States of America

E-mail: ag1@uga.edu

Abstract

We propose a theoretical approach to some of the nanorod-based metamaterial implementations that does not depend on macroscopic electrodynamics. The approach is motivated by the fact that in actual experiments the incident electromagnetic wave encounters a metamaterial structure which is planar in its shape, contains a layer or two of artificially created building blocks, and therefore cannot be regarded as a three-dimensional continuous medium. This leads to a theoretical framework in which the phenomenological concept of refractive index loses its principled meaning, and the deeper concept of scattering is taking center stage. Our proposal and its mathematical realization rely heavily on Feynman's explanation of the physical origin of the index of refraction and on his formula for the field of a plane of oscillating charges. We provide a complete proof of Feynman's formula, filling in some steps that were missing in the original derivation, and then generalize it to the case of a finite disk, which may be relevant to the actual experiments involving laser beams. We then show how the formula can be applied to metamaterial nanoplasmonics by considering some subtle interference effects in uniform laser beams striking metamaterial plates. The first two effects use a single layer of aligned plasmonic nanorods, while the third uses a single layer of gyrotropic elements that may conveniently be described by the celebrated Born-Kuhn oscillator model. The considered effects can potentially be used in the development of quality standards for various metamaterial devices.

1. Introduction

Maxwell's classical electrodynamics [1], the pinnacle of 19th century theoretical physics, supplemented by Lorentz' electron theory of matter [2, 3] require for their mutual conceptual consistency the existence of three clearly distinguishable length scales [4, 5]. Each scale comes equipped with its own characteristic distance (as well as the associated volume element) that has very specific physical meaning. The first, *microscopic* scale operates at the level of the fundamental structural elements of a given medium (atoms, molecules, etc.), where, depending on the context, the characteristic distance, d_1, represents either the typical size of the fundamental element or the separation distance between two nearest such elements. The second, *intermediate* scale defines the size of the so-called 'physical infinitesimally small volume' [4, 6] over which the macroscopic averaging of various field quantities has to be performed. Its characteristic distance, d_2, corresponds to the size of an ideal probe that could be used to measure the field in a given experimental situation [3, 7]. The third, *macroscopic* scale, d_3, characterizes the macroscopic volume in which the *continuous* (that is, macroscopically averaged) fields are actually defined. The standard example is provided by a plane electromagnetic wave of wavelength λ propagating in a transparent medium, in which case d_1 is the separation distance between the molecules, d_3 is on the order of the wavelength, and d_2 is some distance that satisfies the strong inequality, $d_1 \ll d_2 \ll d_3$.

Of the three scales mentioned above, the intermediate scale occupies a very peculiar position. Its characteristic distance has to be sufficiently small for the measurement process to provide the detailed description of the system at hand (say, provide the field values in the region which is several wavelengths long),

and yet it has to be sufficiently large for the associated characteristic volume to contain a great number of microscopic structural elements for the averaging procedure to be meaningful. Oftentimes, the d_2 is not even explicitly mentioned or discussed, or its justification is sketchy and hand-waving, which makes the presence of the intermediate scale either ambiguous or not immediately clear. In spite of all these imperfections in its definition, whenever one deals with a medium that is regarded as continuous, the intermediate scale must always unreservedly be present. Its very existence, no matter how hypothetical, is absolutely indispensable for any 'legitimate' use of continuous electrodynamics. This rather stringent requirement stems from the epistemological position that, since Maxwell's equations describe experimentally measurable quantities, there should exist a practically realizable method of their determination.

On the other hand, we know from everyday experience that too strict adherence to operational definitions is not at all necessary for the productive development of a theory. Two very instructive examples immediately come to mind, although they are not directly related to the topic under consideration. The first of them is the discovery by Dirac [8] of his famous wave equation for the electron in which there appeared some mysterious matrices that had no immediate physical interpretation (due to the presence of 'additional' components and indirect relation to the velocity operator). Another example is the experimental interpretation of the eigenvalues of the position operator for an electron in a hydrogen atom. To determine electron's position one has to strike the atom with highly energetic photons which would destroy the atom, a procedure similar to the one reported in [9] in which the authors used photoionization and an electrostatic lens to directly observe the electron orbitals. So even though the system in question would be destroyed by the actual measurement, one still uses the quantum mechanical language of wave functions and position operators to describe it.

When we turn our attention to metamaterial electrodynamics, we encounter a similar dichotomy. Often, metamaterial structures consist of just a few layers of artificially created building blocks and therefore cannot be regarded as three-dimensional continuous media for the purpose of macroscopic averaging. There is no concept of intermediate scale here, since the entire width of the system is comparable to the size of the 'microscopic' structural element. Nevertheless, when applied to such artificial noncontinuous structures, macroscopic electrodynamics (together with the standard procedures for retrieval of effective material parameters [10–14]) seems to be working remarkably well in predicting system's electromagnetic properties [12, 15–21]; so much so that one can't help wondering if something deep is at play here underlying the theory's success. These considerations naturally lead to the question of why macroscopic electrodynamics relates so well to metamaterial systems in general, and nanoplasmonic ones in particular. It seems intuitively obvious that at the fundamental level the concept of scattering should play a major role in answering this important question. One needs to decide, however, which specific approach to scattering to take and how much rigor to exercise. Much of past work involved accurate and detailed studies of scattering on individual structural elements, taking into account some nontrivial near-field effects, followed by careful statistical averaging to describe the corresponding effective medium that would mimic system's electromagnetic response (see, e. g., [22–27]). Here we propose an approach —somewhat less detailed, but also rooted in scattering and capable of providing some deep physical insight— to systems in which individual plasmonic nanorods (or their simple combinations) play the role of fundamental structural elements. We are primarily interested in either single sheets of aligned nanorods or metamaterial plates made of corner-stacked nanorods, which we propose to model—and this is our main idea—as *planes of oscillating charges*. This approach, whose details will be elucidated below, goes back to Feynman and is based on his formula for the field of a plane of oscillating charges, to which we now turn.

2. Derivation of Feynman's formula for the field of a plane of oscillating charges

2.1. Preliminary considerations

We assume the reader is familiar with Feynman's semi-intuitive derivation of his formula for the field of a plane of oscillating charges (see equations (9) and (24) below) as presented in [28]. The derivation misses some important steps which we aim to fill in here first, before discussing some applications in nanoplasmonics.

The importance of Feynman's formula stems from its use in explaining the physical origin of the refractive index of a dielectric medium whose underlying structural elements (e. g., atoms) may conveniently be described by the Drude-Lorentz oscillator model. To show how light 'slows down' in a dielectric material, Feynman ([28], Ch. 31) treats the field of the transmitted electromagnetic wave as consisting of two parts: the original (incoming) wave and the radiation field of all harmonically driven charges comprising the material. He then subdivides the charges into a great number of planar sheets and asks for the contribution by one such sheet, at which point the formula for the field of an oscillating plane naturally enters the discussion. In Feynman's analysis the dielectric material is not regarded as a medium *per se*, but as a large collection of charged particles sprinkled around and scattering light *in a vacuum*, with *all* the fields propagating with the *same* limiting speed, c. The apparent
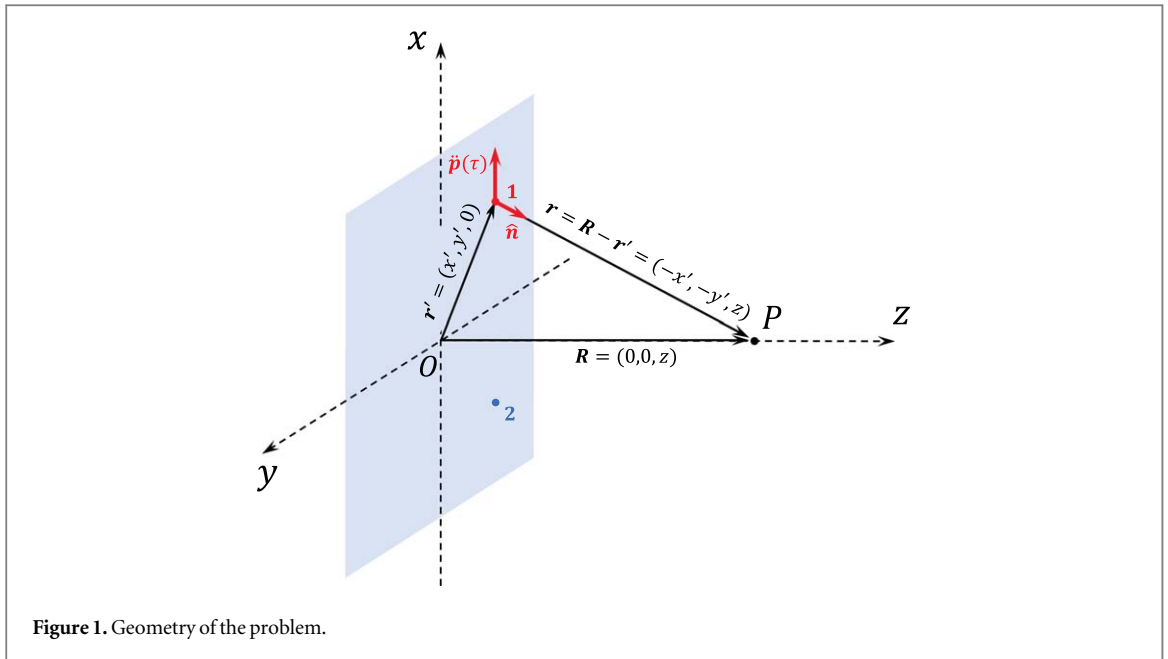
Figure 1. Geometry of the problem.

reduction in that speed then turns out to be nothing but an interference effect, a mathematical fluke, mathematical curiosity.

Since each oscillating charge can be regarded as an oscillating dipole, $\boldsymbol{p}$, we begin our derivation of Feynman's formula with the *exact* expression for the field of a radiating point dipole valid at any distance, r, regardless of the wavelength, λ (Coulomb's constant dropped for notational simplicity and will be restored later; overdots indicate differentiation with respect to time),

$$\boldsymbol{E}^{(\text{dipole})}(P,\,t) = \frac{3(\boldsymbol{p}(\tau)\cdot\hat{\boldsymbol{n}})\hat{\boldsymbol{n}} - \boldsymbol{p}(\tau)}{r^3} + \frac{3(\dot{\boldsymbol{p}}(\tau)\cdot\hat{\boldsymbol{n}})\hat{\boldsymbol{n}} - \dot{\boldsymbol{p}}(\tau)}{cr^2} + \frac{(\ddot{\boldsymbol{p}}(\tau)\cdot\hat{\boldsymbol{n}})\hat{\boldsymbol{n}} - \ddot{\boldsymbol{p}}(\tau)}{c^2r}, \quad \tau = t - \frac{r}{c}. \quad (1)$$

According to (1), in the far zone, the electric field vector $\boldsymbol{E}(P, t)$ evaluated at the observation point $P = (x, y, z)$ at time t is orthogonal to vector $\boldsymbol{r}$ connecting the dipole to P and lies in the plane spanned by $\boldsymbol{r}$ and $\ddot{\boldsymbol{p}}(\tau)$, evaluated at the retarded time τ (with similar interpretations for the near and induction terms). In our problem all dipoles are assumed to be coherently oscillating in the xy-plane in the direction parallel to the x-axis, as shown in figure 1. Correspondingly, for points $P = (0, 0, z)$ located on the z-axis, all relevant vectors have components as indicated in that figure, with $\boldsymbol{p}(\tau) = (p_x(\tau), 0, 0)$, $\ddot{\boldsymbol{p}}(\tau) = (\ddot{p}_x(\tau), 0, 0)$, and

$$\hat{\boldsymbol{n}} = \frac{\boldsymbol{r}}{r} = \frac{(-x', -y', z)}{\sqrt{x'^2 + y'^2 + z^2}}. \quad (2)$$

Substitution into (1) gives,

$$\boldsymbol{E}^{(\text{dipole})}(z,\,t) = p_x(\tau)\frac{(2x'^2 - y'^2 - z^2,\ 3x'y',\ -3x'z)}{(x'^2 + y'^2 + z^2)^{5/2}}$$

$$+ \frac{\dot{p}_x(\tau)}{c}\frac{(2x'^2 - y'^2 - z^2,\ 3x'y',\ -3x'z)}{(x'^2 + y'^2 + z^2)^2}$$

$$+ \frac{\ddot{p}_x(\tau)}{c^2}\frac{(-y'^2 - z^2,\ x'y',\ -x'z)}{(x'^2 + y'^2 + z^2)^{3/2}}, \quad (3)$$
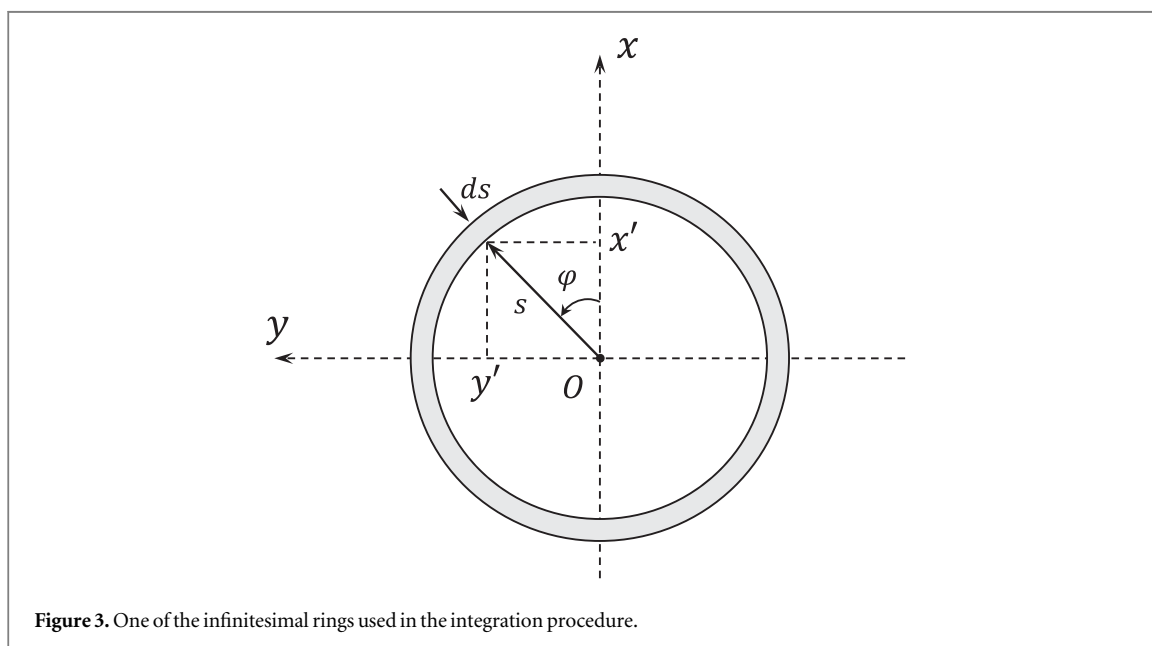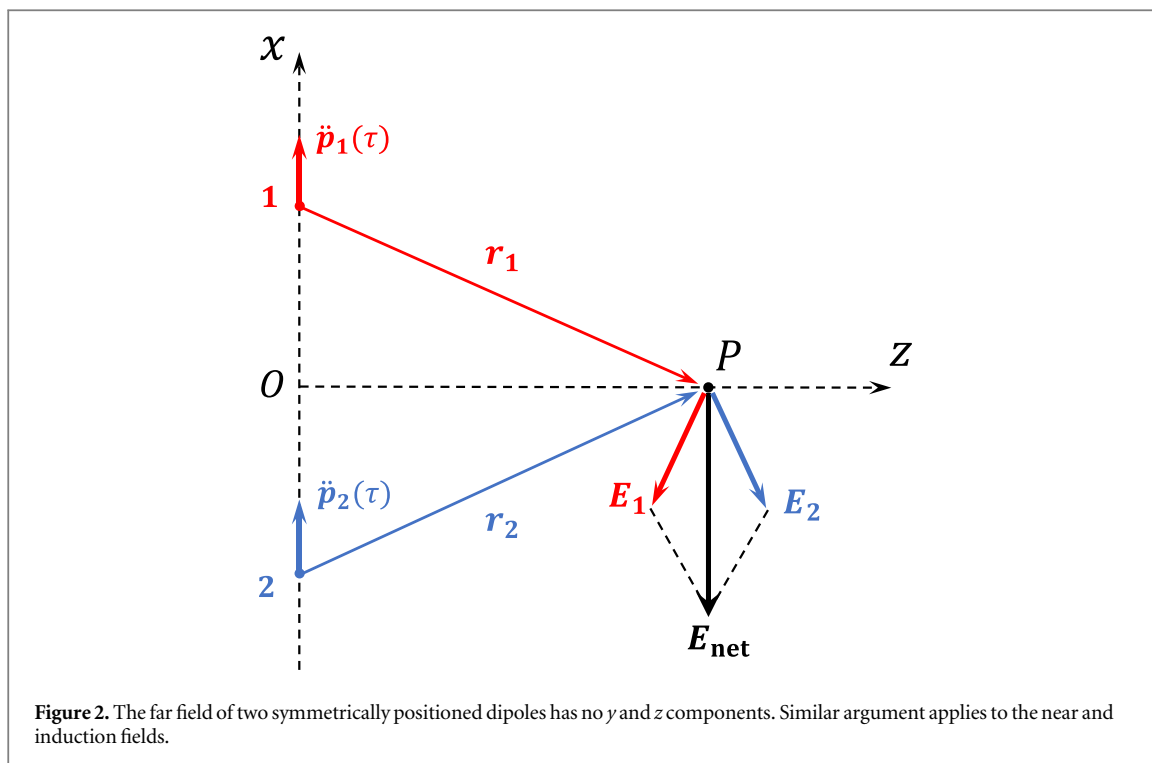
which shows that the y and z components of the electric field change sign under the $x' \leftrightarrow -x'$ transformation. This means that they vanish for any distribution of charges symmetric with respect to the y-axis, which can be understood intuitively by sketching the net field due to a pair of identical dipoles positioned symmetrically relative to the y-axis, with one directly above the other (figure 2).

Therefore, only the x component of the field,

$$E_x^{(\text{dipole})}(z,\,t) = p_x(\tau)\frac{2x'^2 - y'^2 - z^2}{(x'^2 + y'^2 + z^2)^{5/2}} + \frac{\dot{p}_x(\tau)}{c}\frac{2x'^2 - y'^2 - z^2}{(x'^2 + y'^2 + z^2)^2} - \frac{\ddot{p}_x(\tau)}{c^2}\frac{y'^2 + z^2}{(x'^2 + y'^2 + z^2)^{3/2}}, \quad (4)$$

needs to be kept in our derivation.

The calculation of the total field then proceeds by dividing the planar distribution into a series of infinitesimally thin concentric rings of variable radii s and thickness ds, and then integrating (figure 3).

Figure 2. The far field of two symmetrically positioned dipoles has no y and z components. Similar argument applies to the near and induction fields.

Figure 3. One of the infinitesimal rings used in the integration procedure.

For one such ring we have, on the basis of (4) and using $x' = s \cos \varphi$, $y' = s \sin \varphi$,

$$
\begin{aligned}
E_x^{(\mathrm{ring})}(z, t) = {} & \eta \, p_x(\tau) \int_0^{2\pi} \frac{2s^2 \cos^2 \varphi - s^2 \sin^2 \varphi - z^2}{(s^2 + z^2)^{5/2}} s \, d\varphi \, ds \\
& + \frac{\eta \, \dot{p}_x(\tau)}{c} \int_0^{2\pi} \frac{2s^2 \cos^2 \varphi - s^2 \sin^2 \varphi - z^2}{(s^2 + z^2)^2} s \, d\varphi \, ds \\
& - \frac{\eta \, \ddot{p}_x(\tau)}{c^2} \int_0^{2\pi} \frac{s^2 \sin^2 \varphi + z^2}{(s^2 + z^2)^{3/2}} s \, d\varphi \, ds,
\end{aligned}
\tag{5}
$$

where η is the surface density (the number of dipoles per unit area). Taking into account that $\int_0^{2\pi} \cos^2 \varphi \, d\varphi = \int_0^{2\pi} \sin^2 \varphi \, d\varphi = \pi$, $r^2 = s^2 + z^2$, $s \, ds = r \, dr$, we get

$$E_x^{(\text{ring})}(z,\,t) = \pi\,\eta\left\{p_x(\tau)\,\frac{1}{r^2}\left(1 - \frac{3z^2}{r^2}\right) + \frac{\dot{p}_x(\tau)}{c}\,\frac{1}{r}\left(1 - \frac{3z^2}{r^2}\right) - \frac{\ddot{p}_x(\tau)}{c^2}\left(1 + \frac{z^2}{r^2}\right)\right\}dr, \tag{6}$$

which, for harmonically oscillating charges with

$$p_x(\tau) = qx_0 e^{-i\omega(t-r/c)}, \tag{7}$$

results in the *total* field,

$$E_x(z,\,t) = \pi\eta qx_0\,e^{-i\omega t}\,I(z,a), \quad I(z,a) \equiv \int_z^a e^{i(\omega/c)r}\left[\frac{1}{r^2}\left(1 - \frac{3z^2}{r^2}\right) - \frac{i\omega}{c}\,\frac{1}{r}\left(1 - \frac{3z^2}{r^2}\right) + \frac{\omega^2}{c^2}\left(1 + \frac{z^2}{r^2}\right)\right]dr. \tag{8}$$

In the above we used quantum mechanical sign convention for frequency ω and kept the upper limit of integration, *a*, finite with the intention of distinguishing between two interesting cases: an infinite plane (in which case $a \to \infty$) and a disk (in which case *a* remains finite). Before proceeding further, let us take a brief look at Feynman's own derivation.

2.2. Brief review of Feynman's 'proof'
Feynman derived his result (see section 30-7 in [28]),

$$E_x(P) = 2\pi\,\frac{\eta q}{c}\,i\omega x_0 e^{-i\omega(t-z/c)}, \tag{9}$$

by working in the far zone and using the approximate dipole radiation formula,

$$E_x^{(\text{dipole})}(P) \approx \frac{q}{c^2 r}\,\omega^2 x_0\,e^{-i\omega(t-z/c)}, \tag{10}$$

which represents the field in dipole's equatorial plane only, thus ignoring the near zone, the induction zone, and the angular dependence due to mutual orientation of $\ddot{\boldsymbol{p}}(\tau)$ and $\hat{\boldsymbol{n}}$ in the far zone (*cf*. our equation (4)). This leads to the expression for the total field,

$$E_x(P) = 2\pi\eta qx_0\,e^{-i\omega t}\,\frac{\omega^2}{c^2}\int_z^a e^{i(\omega/c)r}\,dr, \tag{11}$$

which differs substantially from our equation (8). In the limit $a \to \infty$ the integral in (11) evaluates to

$$\int_z^\infty e^{i(\omega/c)r}\,dr = -i\frac{c}{\omega}[e^{i(\omega/c)\infty} - e^{i(\omega/c)z}], \tag{12}$$

which is not well defined. To make sense of the infinite exponent, Feynman regularizes (11) by replacing the constant surface density η with radially *tapered* density $\eta(r)$ and then evaluating the integral,

$$\int_z^\infty \eta(r)\,e^{i(\omega/c)r}\,dr \approx \sum_j \eta(r_j)\,e^{i(\omega/c)r_j}\,\Delta r_j$$

$$= \eta(z)\,e^{i(\omega/c)z}\,\Delta r + \eta(z+\Delta r)\,e^{i(\omega/c)(z+\Delta r)}\,\Delta r + \eta(z+2\Delta r)\,e^{i(\omega/c)(z+2\Delta r)}\,\Delta r + ...$$

$$= \eta(z)\,e^{i(\omega/c)z}\left\{\Delta r + \Delta r\,\frac{\eta(z+\Delta r)}{\eta(z)}\,e^{i(\omega/c)\Delta r} + \Delta r\,\frac{\eta(z+2\Delta r)}{\eta(z)}\,e^{2i(\omega/c)\Delta r} + ...\right\}, \tag{13}$$

graphically by adding up small arrows of slowly decreasing length that represent the complex-valued terms in the curly brackets of the Riemann sum above. By depicting this process in figure 4 we immediately see that the integral is equal to $i(c/\omega)\eta(z)\,e^{i(\omega/c)z}$, which corresponds to setting the infinite exponent in equation (12) to zero, thus recovering equation (9).

2.3. Derivation continued
We now return to our expression (8) and regularize it à la Feynman by replacing the constant density η with the tapered one which we choose to be in the form,

$$\eta(r) = \eta e^{-\alpha(\omega/c)r}, \quad \alpha > 0, \tag{14}$$

where α is a small positive parameter to be set to zero at the end of the calculation. This gives,

$$I(z,a) = \int_z^a e^{(i-\alpha)(\omega/c)r}\left\{\frac{\omega^2}{c^2} - \frac{i\omega}{c}\,\frac{1}{r} + \left(1 + \frac{\omega^2 z^2}{c^2}\right)\frac{1}{r^2} + \frac{3i\omega z^2}{c}\,\frac{1}{r^3} - \frac{3z^2}{r^4}\right\}dr, \tag{15}$$

which allows us to interpret Feynman's regularization procedure as Wick rotation in the complex *r*-plane (see also figure 6 and equation (22) below). Next,

Figure 4. Feynman's approach to evaluating $\int_z^\infty \eta(r)\, e^{i(\omega/c)r}\, dr$ with the help of a radially tapered surface density $\eta(r)$ as given in equation (13).
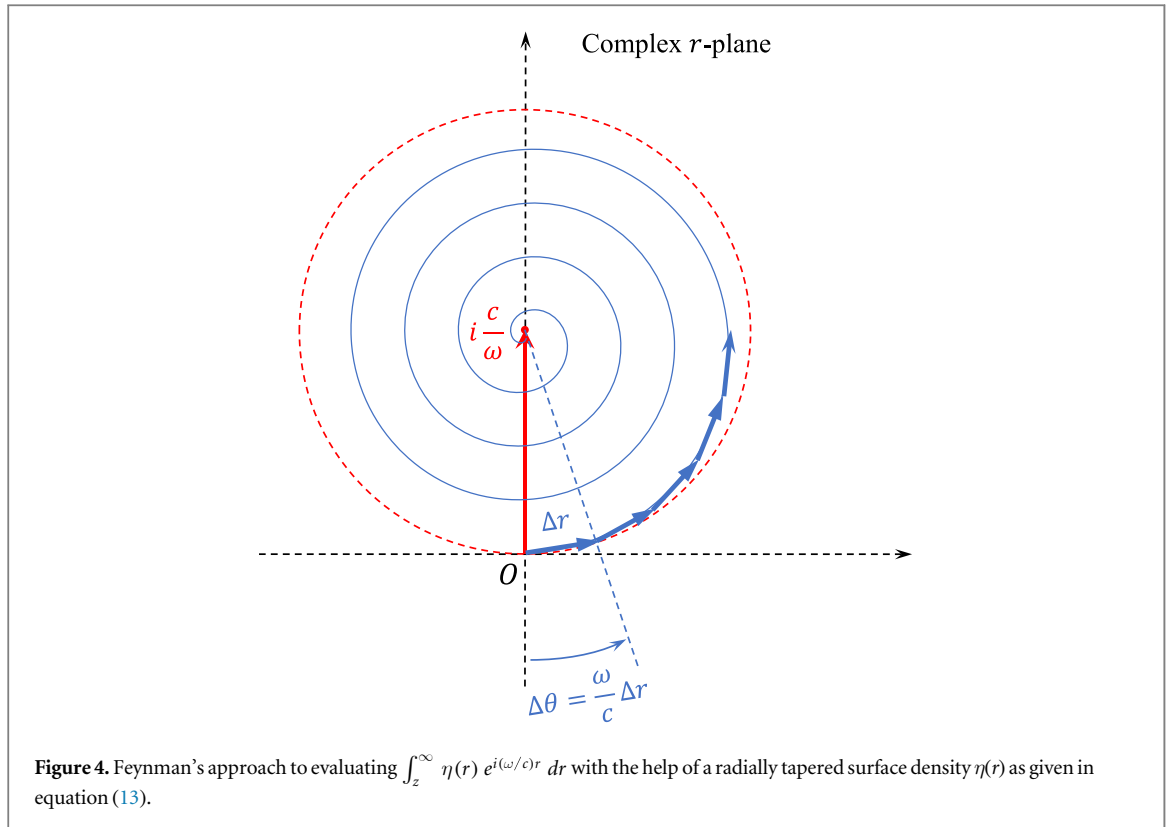
$$I(z, a) = \frac{\omega}{(i - \alpha)c}(e^{\xi_2} - e^{\xi_1}) - \frac{i\omega}{c}\int_{\xi_1}^{\xi_2} \frac{e^\zeta}{\zeta}\, d\zeta + \left(1 + \frac{\omega^2 z^2}{c^2}\right)(i - \alpha)\frac{\omega}{c}\int_{\xi_1}^{\xi_2} \frac{e^\zeta}{\zeta^2}\, d\zeta$$

$$+ \frac{3i\omega z^2}{c}\left[(i - \alpha)\frac{\omega}{c}\right]^2 \int_{\xi_1}^{\xi_2} \frac{e^\zeta}{\zeta^3}\, d\zeta - 3z^2\left[(i - \alpha)\frac{\omega}{c}\right]^3 \int_{\xi_1}^{\xi_2} \frac{e^\zeta}{\zeta^4}\, d\zeta, \tag{16}$$

where

$$\xi_2 = (i - \alpha)(\omega/c)a, \quad \xi_1 = (i - \alpha)(\omega/c)z. \tag{17}$$

Taking into account that

$$\int_{\xi_1}^{\xi_2} \frac{e^\zeta}{\zeta^2}\, d\zeta = \int_{\xi_1}^{\xi_2} \frac{e^\zeta}{\zeta}\, d\zeta - \frac{e^\zeta}{\zeta}\bigg|_{\xi_1}^{\xi_2},$$

$$\int_{\xi_1}^{\xi_2} \frac{e^\zeta}{\zeta^3}\, d\zeta = \frac{1}{2}\left\{\int_{\xi_1}^{\xi_2} \frac{e^\zeta}{\zeta}\, d\zeta - \left[\frac{e^\zeta}{\zeta} + \frac{e^\zeta}{\zeta^2}\right]_{\xi_1}^{\xi_2}\right\},$$

$$\int_{\xi_1}^{\xi_2} \frac{e^\zeta}{\zeta^4}\, d\zeta = \frac{1}{2 \cdot 3}\left\{\int_{\xi_1}^{\xi_2} \frac{e^\zeta}{\zeta}\, d\zeta - \left[\frac{e^\zeta}{\zeta} + \frac{e^\zeta}{\zeta^2} + \frac{2e^\zeta}{\zeta^3}\right]_{\xi_1}^{\xi_2}\right\}, \tag{18}$$

and

$$\int_{\xi_1}^{\xi_2} \frac{e^\zeta}{\zeta}\, d\zeta = \text{Ei}(\xi_2) - \text{Ei}(\xi_1), \tag{19}$$

after some algebra we find,

$$I(z, a) = e^{(i-\alpha)(\omega/c)a}\left[\frac{\omega}{(i - \alpha)c} - \frac{1}{a}\left(1 - \frac{z^2}{a^2} + \frac{(\alpha + 2i)\omega z^2}{2ac} - \frac{\alpha(\alpha + i)\omega^2 z^2}{2c^2}\right)\right]$$

$$- \frac{\omega}{2c}\frac{e^{(i-\alpha)(\omega/c)z}}{(i - \alpha)}\left((4 + \alpha(\alpha + i)) - \alpha(\alpha^2 + 1)\frac{\omega z}{c}\right)$$

$$- \frac{\alpha\omega}{c}\left(1 - (\alpha^2 + 1)\frac{\omega^2 z^2}{2c^2}\right)\left(\text{Ei}\left[(i - \alpha)\frac{\omega}{c}a\right] - \text{Ei}\left[(i - \alpha)\frac{\omega}{c}z\right]\right), \tag{20}$$
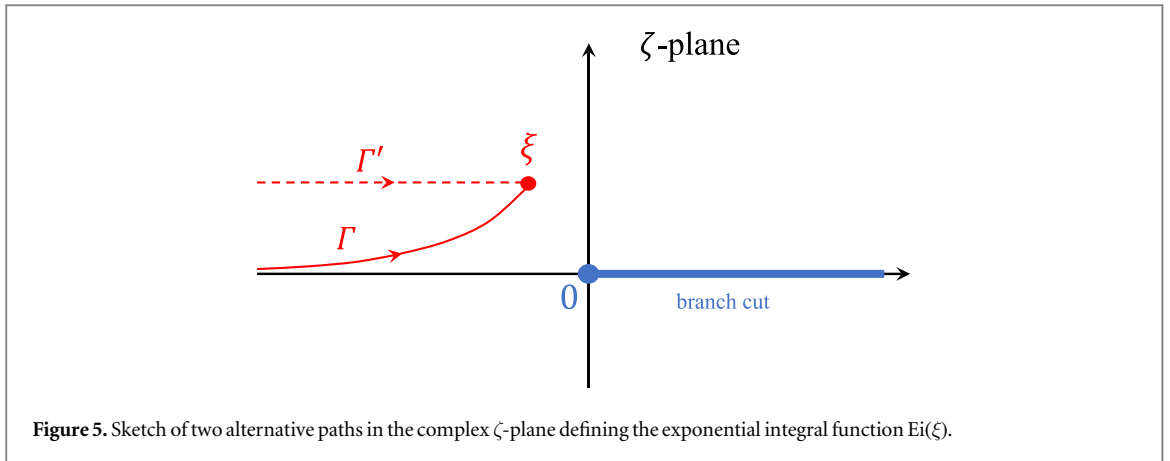
Figure 5. Sketch of two alternative paths in the complex ζ-plane defining the exponential integral function Ei(ξ).

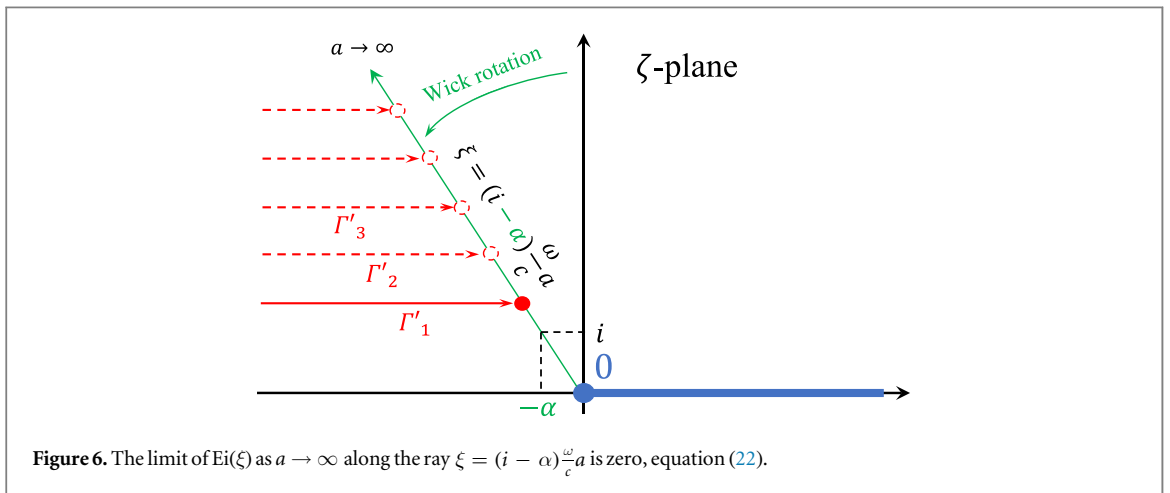**Figure 6.** The limit of Ei(ξ) as $a \to \infty$ along the ray $\xi = (i - \alpha)\frac{\omega}{c}a$ is zero, equation (22).

where Ei(ξ) is the well-known exponential integral [29],

$$\text{Ei}(\xi) = \int_{-\infty}^{\xi} \frac{e^{\zeta}}{\zeta}\, d\zeta, \quad |\arg(-\xi)| < \pi. \tag{21}$$

The restriction on the argument is due to the standard choice of the branch cut that makes the integral single-valued (figure 5).

We can view Ei(ξ) as accumulation function for $f(\zeta) = e^{\zeta}/\zeta$ along a path (call it Γ) running from $-\infty$ to ξ in the complex ζ-plane. The choice of this defining path is not unique. One may deform the path arbitrarily as long as it originates at the 'left' infinity and does not cross the branch cut. A simple example is provided by the semi-infinite straight segment Γ' that runs parallel to the real axis and is described by $-\infty < \text{Re}(\zeta) \leqslant \text{Re}(\xi)$, $\text{Im}(\zeta) = \text{Im}(\xi)$. Based on this observation we can see that the limit of Ei(ξ) as $\xi \to \infty$ along the ray shown in figure 6 is equal to zero,

$$\lim_{a \to \infty} \text{Ei}\left[(i - \alpha)\frac{\omega}{c}a \right] = 0. \tag{22}$$

With this result at hand, we are ready to complete our derivation (see equations (8) and (20)).

2.4. Infinite plane

In the case of infinite plane we take the double-limit in (20) using (22) by first letting $a \to \infty$ and then $\alpha \to 0$. This immediately gives,

$$I = 2i\frac{\omega}{c}e^{i(\omega/c)z}, \tag{23}$$

whose use in (8) recovers Feynman's formula,

$$E_x(z, t) = 2\pi \frac{\eta q}{c} i\omega x_0 e^{-i\omega(t - z/c)} \quad \text{(infinite plane)}. \tag{24}$$
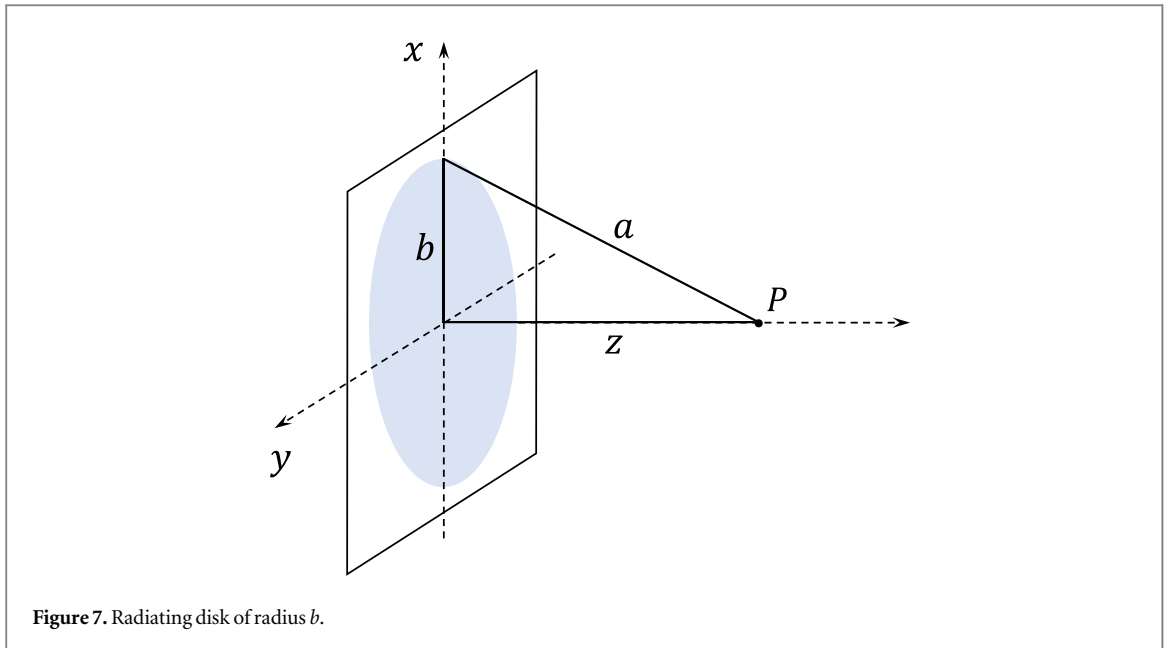
Figure 7. Radiating disk of radius b.

2.5. Finite disk

In the case of a finite disk (of radius b) we set $\alpha = 0$ in (20), keeping a and z finite, as shown in figure 7. This gives,

$$E_x(z,\,t) = 2\pi\frac{\eta q}{c}i\omega x_0\ e^{-i\omega(t-z/c)}\ \mathcal{A}(z), \quad \mathcal{A}(z) = 1 - \frac{1}{2}\left(1 + \frac{z^2}{a^2} - \frac{ic}{\omega a}\frac{b^2}{a^2}\right)e^{i(\omega/c)(a-z)}, \quad a = \sqrt{z^2\ +\ b^2}, \tag{25}$$

which is valid everywhere on the symmetry axis. Notice that this expression vanishes in the limit $z \to \infty$ (via $\mathcal{A} \to 0$). Also, in the limit $b \to \infty$ we get equation (24) for the infinite plane, provided we formally set $e^{i\infty}$ in $\mathcal{A}$ to zero.

For the far field, with $\lambda/z \ll 1$, $b/z \ll 1$ (with no additional restriction on b), using approximation $a \approx z$ $(1 + b^2/(2z^2))$ we get,

$$E_x(z,\,t) = 2\pi\frac{\eta q}{c}i\omega x_0 e^{-i\omega(t-z/c)}\ \mathcal{A}(z), \quad \mathcal{A}(z) = 1 - e^{i\pi b^2/(\lambda z)}, \tag{26}$$

and the corresponding (unnormalized) intensity,

$$|\mathcal{A}(z)|^2 = 2\left[1 - \cos\left(\frac{\pi b^2}{\lambda z}\right)\right], \tag{27}$$

where πb^2 is the area of the disk. If, in addition, we impose a stronger condition $b^2/(\lambda z) \ll 1$, we recover the intuitively anticipated result,

$$E_x(z,\,t) = 2\pi\frac{\eta q}{c}i\omega x_0 e^{-i\omega(t-z/c)}\ \mathcal{A}(z), \quad \mathcal{A}(z) = -i\frac{\pi b^2}{\lambda z}, \quad |\mathcal{A}(z)|^2 = \left(\frac{\pi b^2}{\lambda z}\right)^2, \tag{28}$$

or,

$$E_x(z,\,t) = \frac{Q}{c^2 z}\omega^2 x_0\ e^{-i\omega(t-z/c)}, \quad Q = \pi b^2 \eta q, \tag{29}$$

for a 'point-like' disk of total charge Q viewed from a very large distance. The predicted intensity of disk's field, $|\mathcal{A}(z)|^2$, as the function of the distance, z, in a realistic experimental regime described by equation (26) is shown in figures 8 and 9.

It is interesting to notice that for distances $z > z_0 \equiv b^2/\lambda$ the radiation intensity ceases to oscillate. This corresponds to the condition (see figure 7),

$$\frac{\Delta\ell}{\lambda} \equiv \frac{a-z}{\lambda} \approx \frac{b^2}{2\lambda z} \equiv \frac{z_0}{2z} < 1, \tag{30}$$

in which case the path length difference, $\Delta\ell = a - z$, between the outermost and central dipoles is less than the wavelength λ for any such z. This results in a very slow change of the interference pattern with distance, which makes the 'last' oscillation of combined intensity 'stretch out' all the way to spatial infinity ($z \to \infty$ in figure 8).

Figure 8. Blue curves: predicted behavior of the radiation intensity, $|\mathcal{A}(z)|^2$ (*on the symmetry axis*, at points $P = (0, 0, z)$), as the function of the distance, z, from a uniform disk of identical oscillating dipoles, as described by equation (26). Here, $\lambda = 632.8$ nm is the radiation wavelength and b is the radius of the disk. Orange curves: asymptotic behavior of $|\mathcal{A}(z)|^2$ at large z, as given by equations (28) and (29). Compare with figure 9.

Before concluding this section, let us make a mental note that the expression for the field given by Feynman's formula is proportional to the retarded *velocity* of the oscillating charges, or, equivalently, to the corresponding retarded electric *current*. The appearance of the current is not too surprising and may be traced to a more traditional approach to scattering on two-dimensional structures, as we briefly outline in appendix A. When we come to discuss electrodynamics of chiral media, this result, properly generalized, will play a central role in connecting our theory to the previously published work on metamaterial nanoplasmonics. Such connection is possible because within the Born-Kuhn model of optical activity the very definition of optical rotatory dispersion is given in terms of the bound *currents* induced in the material by the incident electromagnetic wave (see, e. g., discussion in [30]).

Figure 9. Radiation intensity, $|\mathcal{A}(z)|^2$, in the *xz*-plane, as the function of the distance, *z*, from a uniform disk of identical oscillating dipoles, found by numerical integration of equation (1). Here, $\lambda = 632.8$ nm is the radiation wavelength and $b = 1$ mm is the radius of the disk, so that $z_0 \equiv b^2/\lambda = 1.58028$ m. (In the *yz*-plane the plot is identical, and in any other plane is similar, to this one.)
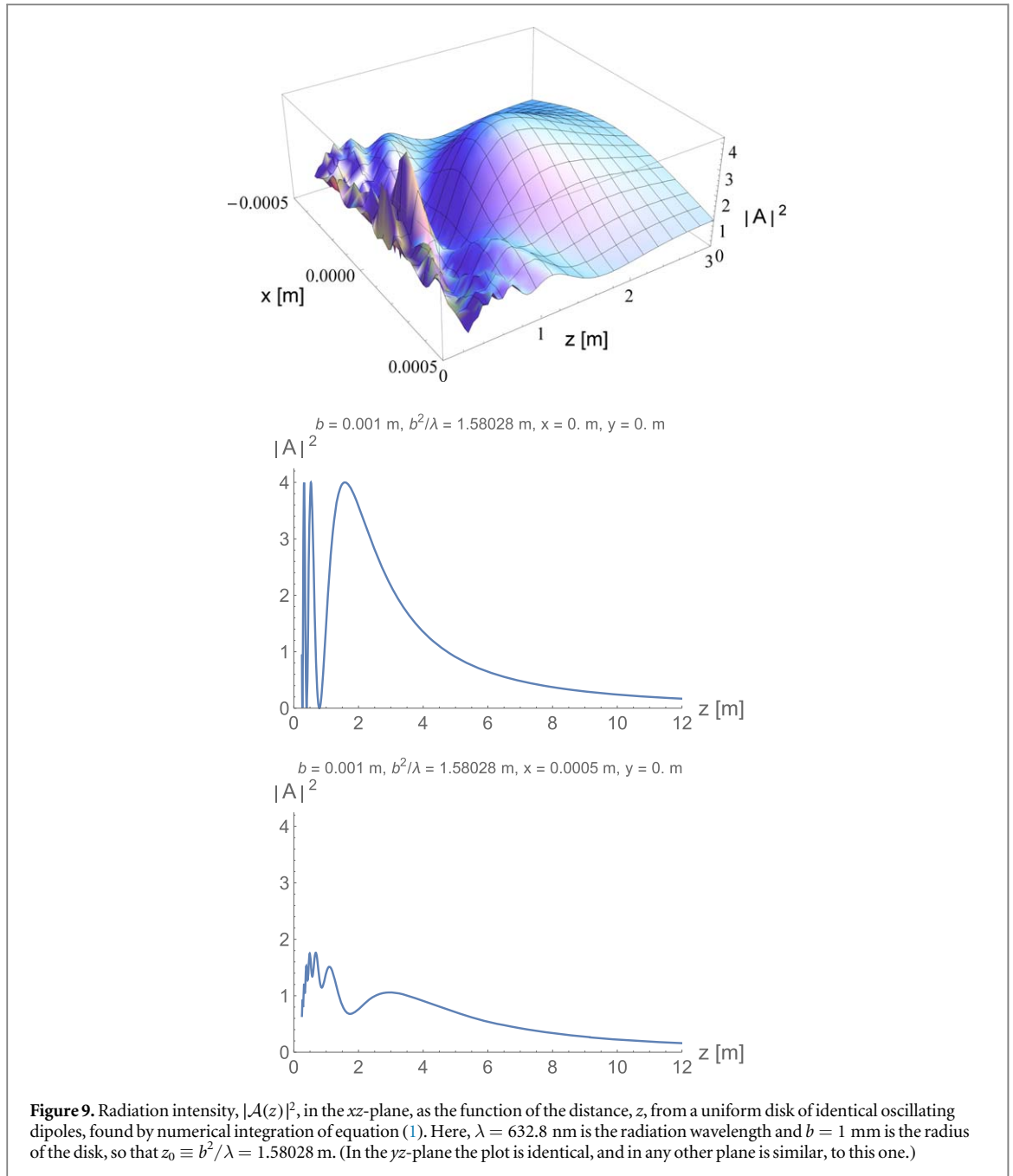
3. Applications in metamaterial nanoplasmonics

3.1. Laser beam striking a sheet of aligned plasmonic nanorods

Assume now that the radiating disk of finite radius *b* is artificially induced by a *uniform* laser beam of wavelength $\lambda = 632.8$ nm (He–Ne laser, red) and cross-sectional radius $b = 1$ mm striking infinitesimally thin sheet of dipoles, such as a layer of plasmonic nanorods, as depicted in figure 10. Assume also that the observation point *P* is chosen, say, anywhere between 0.25 to 6.5 meters from the sheet. In that case,

$$\omega b/c \;=\; 2\pi b/\lambda = 2\pi \times 1580, \tag{31}$$

and

$$0.00015 < b/z < 0.004, \quad 0.24 < b^2/(\lambda z) < 6.3, \quad b^2/\lambda = 1.58 \text{ m}, \tag{32}$$

so we are in the experimental situation described by equation (26). For Implementation I, in which the field measurements are made in the reflected beam, the predicted intensity, $|\mathcal{A}(z)|^2$, as the function of the distance, *z*, is given in figure 8 (provided we work at nearly normal incidence).

Despite the high sensitivity of the intensity pattern to the values of the beam's diameter, the proposed setup seems to be within an easily realizable range of experimental parameters, which should make the observation of

Figure 10. Schematics of the experiment in which radiating disk of oscillating dipoles is effectively generated by a laser beam that either (I) is scattered (at nearly normal incidence) by, or (II) passes through, a two-dimensional sheet of aligned plasmonic nanorods.
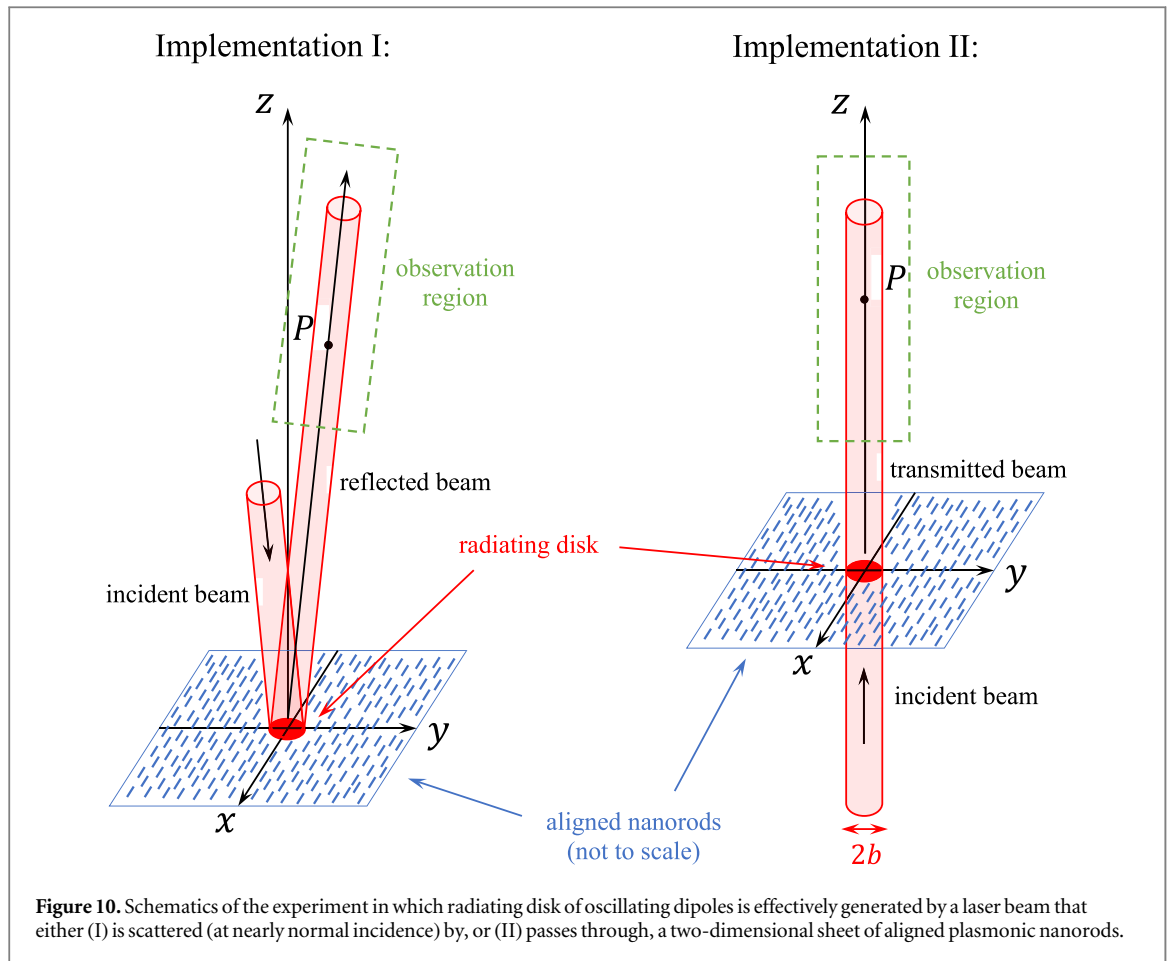
this interference effect relatively straightforward. [We note in passing that the reason for using metallic systems, rather than, say, dielectric ones, is not a matter of principle (our theory is equally applicable to dielectric systems as well), but the practical one. Because of very high density of quasi-valence electrons, the induced electric moments in plasmonic nanorods are many orders of magnitude greater than in the dielectric ones, which leads to a much stronger optical response. Typical resonant wavelengths in such systems (usually, gold and silver) are on the order of a few hundred to a couple thousand nanometers [21, 30–36], which can be adjusted by varying nanorod dimensions, allowing experiments at optical to near-infrared frequencies. Here we visualize a simplified scenario in which the nanorods are not too densely packed, potentially missing on some interesting contributions coming from various near field interaction effects (see, e. g., [22, 23]; also appendix A). In addition, since our derivation assumes point-like dipoles, the size, d_1, of the nanorods is restricted by the condition $d_1 \ll \lambda$, which also sets the scale for their separation distance (see discussion around equations (56), (57)). Correspondingly, in experiments described by our theory, d_1 ranges between a few to a few tens nanometers. Packing closer than that would push us into the regime of continuous electrodynamics, rendering our approach inapplicable.]

For Implementation II, in which the field measurements are made in the transmitted beam, the net field at P is the sum of the incoming wave $(\mathcal{E}_x, \mathcal{E}_y)e^{-i\omega(t-z/c)}$ and the radiation field of the oscillating disk. The equation of motion for a driven dipole in this case is

$$\ddot{x} + \gamma\dot{x} + \omega_0^2 x = (q/m)\mathcal{E}_x e^{-i\omega t}, \tag{33}$$

where ω_0 is the natural frequency of the equivalent Drude-Lorentz oscillator, γ is the damping coefficient, and q/m is the charge-to-mass ratio. Denoting

$$\Omega^2 \equiv \omega_0^2 - \omega^2 - i\gamma\omega, \tag{34}$$

we get the steady state solution,

$$x(t) = x_0 e^{-i\omega t}, \quad x_0 = \frac{q}{m\Omega^2}\mathcal{E}_x, \tag{35}$$

which, on the basis of (26), gives the total transmitted field,

$$E_x(z, t) = \mathcal{T}(z)\,\mathcal{E}_x\,e^{-i\omega(t-z/c)}, \quad E_y(z, t) = \mathcal{E}_y\,e^{-i\omega(t-z/c)}, \quad \mathcal{T}(z) \equiv 1 \;+\; i\,\frac{\omega D}{2c}\frac{\omega_{\mathrm{p1}}^2}{\Omega^2}\mathcal{A}(z), \tag{36}$$

where $\mathcal{A} = 1$ for a wide beam and $\mathcal{A}(z) = 1 - e^{i\pi b^2/(\lambda z)}$ for a narrow beam of cross-sectional radius b. In the above, we formally introduced the plasma frequency (with Coulomb's constant restored) for a *single* sheet of nanorods, hence subscript 1 (*cf.* (49)),

$$\omega_{\text{p1}}^2 \equiv \frac{\eta q^2}{\varepsilon_0 m D}, \tag{37}$$

where D is the thickness of the metamaterial plate (practically, nanorod's cross-sectional diameter) and ε_0 is the electric constant. Notice that a single layer of aligned nanorods is functionally equivalent to a birefringent plate. Also notice that the transmission amplitude can be written in a slightly different form,

$$\mathcal{T}(z) = 1 + i\frac{\omega \omega_{\text{p1}}'}{\Omega^2}\mathcal{A}(z), \tag{38}$$

in terms of a different characteristic frequency (primed plasma frequency),

$$\omega_{\text{p1}}' \equiv \frac{\eta q^2}{2\varepsilon_0 m c}, \tag{39}$$

which may be useful in some contexts, though in what follows we will adhere to traditional definition.

The 'usual' theory based on macroscopic electrodynamics is recovered by setting $\mathcal{A} = 1$ (wide beam) and introducing the quantity which we may call the index of refraction (for lack of a better word),

$$n_1 \equiv 1 + \frac{\omega_{\text{p1}}^2}{2\Omega^2}, \tag{40}$$

which for ω far from resonant ω_0 corresponds approximately to the permittivity of the Drude-Lorentz model, $n_1^2 \approx \varepsilon_{\text{DL}} = 1 + \omega_{\text{p1}}^2/\Omega^2$. In the absence of losses ($\gamma = 0$) and for $\omega \ll \omega_0$, the index of refraction is real and positive, so for an x-polarized wave we get,

$$E_x(z, t) = \left(1 + \frac{i\omega(n_1 - 1)D}{c}\right)\mathcal{E}_x\, e^{-i\omega(t - z/c)} \approx \mathcal{E}_x \exp\left\{-i\omega\left[t - \frac{z}{c} - \left(\frac{D}{c/n_1} - \frac{D}{c}\right)\right]\right\}, \tag{41}$$

which shows an increase in the optical path-length due to an effective reduction in phase velocity (from the original c down to c/n_1) when propagating through the plate, in agreement with Feynman's reasoning ([28], Ch. 31). In the case of a narrow laser beam, using $\mathcal{A}(z) = 1 - e^{i\pi b^2/(\lambda z)}$ and assuming $\gamma = 0$ in equation (36), we get for transmitted radiation intensity,

$$|\mathcal{T}(z)|^2 = 1 + 2(n_1 - 1)\frac{\omega D}{c}\sin\left(\frac{\pi b^2}{\lambda z}\right) + 2\left((n_1 - 1)\frac{\omega D}{c}\right)^2\left[1 - \cos\left(\frac{\pi b^2}{\lambda z}\right)\right], \tag{42}$$

which is depicted in figure 11. [If the rods are deposited on a very thin transparent dielectric substrate then an extra term involving the effective $n_{\text{dielectric}}$ of the material should be included in equations (36) and (41) to account for additional increase in the corresponding optical path-length. If a thick substrate is employed then transmitted intensity should be modified using Fresnel's coefficients familiar from continuous electrodynamics.]

3.2. Laser beam striking a chiral plate

The two-dimensional Born-Kuhn (BK) oscillator model [37, 38] (also [39, 40]) represents a chiral block (the fundamental structural element of a chiral medium) by two coupled charged harmonic oscillators, one at $z = 0$ and the other at $z = d$, displaced as depicted in figure 12 and subjected to a plane electromagnetic wave of frequency ω and wave number $k = \omega/c$ propagating with the limiting speed c along the z-axis. The charges are restricted to move in the x and y directions, respectively, in which case their equations of motion are given by

$$\ddot{x} + \gamma\dot{x} + \omega_0^2 x + \omega_c^2 y = (q/m)\mathcal{E}_x e^{-i\omega t},$$
$$\ddot{y} + \gamma\dot{y} + \omega_0^2 y + \omega_c^2 x = (q/m)\mathcal{E}_y e^{-i(\omega t - kd)}, \tag{43}$$

where ω_c is the coupling frequency and $(\mathcal{E}_x, \mathcal{E}_y)$ are the amplitudes of the x and y components of the electric field in the incoming wave. Using the steady state *Ansatz*,

$$x(t) = x_0 e^{-i\omega t}, \qquad y(t) = y_0 e^{-i(\omega t - kd)}, \tag{44}$$

the equations of motion can be written in matrix form,

$$\begin{pmatrix} \Omega^2 & \omega_c^2 e^{ikd} \\ \omega_c^2 e^{-ikd} & \Omega^2 \end{pmatrix}\begin{pmatrix} x_0 \\ y_0 \end{pmatrix} = \frac{q}{m}\begin{pmatrix} \mathcal{E}_x \\ \mathcal{E}_y \end{pmatrix}, \tag{45}$$

Figure 11. Predicted transmitted intensity, $T(z) = |\mathcal{T}(z)|^2$ (unnormalized), as the function of the distance, z, equation (42), for an x-polarized laser beam passing through a sheet of aligned plasmonic nanorods (Implementation II). Beam parameters: $\lambda = 632.8$ nm, $b = 1$ mm, with arbitrarily chosen $(n_1 - 1)\omega D/c = 0.1$ (red curve, corresponding to $\omega_0 > \omega$) and $(n_1 - 1)\omega D/c = -0.1$ (blue curve, corresponding to $\omega_0 < \omega$).

Figure 12. Schematic representation of the fundamental structural element (the 'chiral block') of a gyrotropic metamaterial in accordance with the two-dimensional Born-Kuhn oscillator model. One possible implementation of the model consists of a single layer of such blocks which, in turn, can be visualized as being made of two planes of pair-wise coupled harmonically oscillating charges.
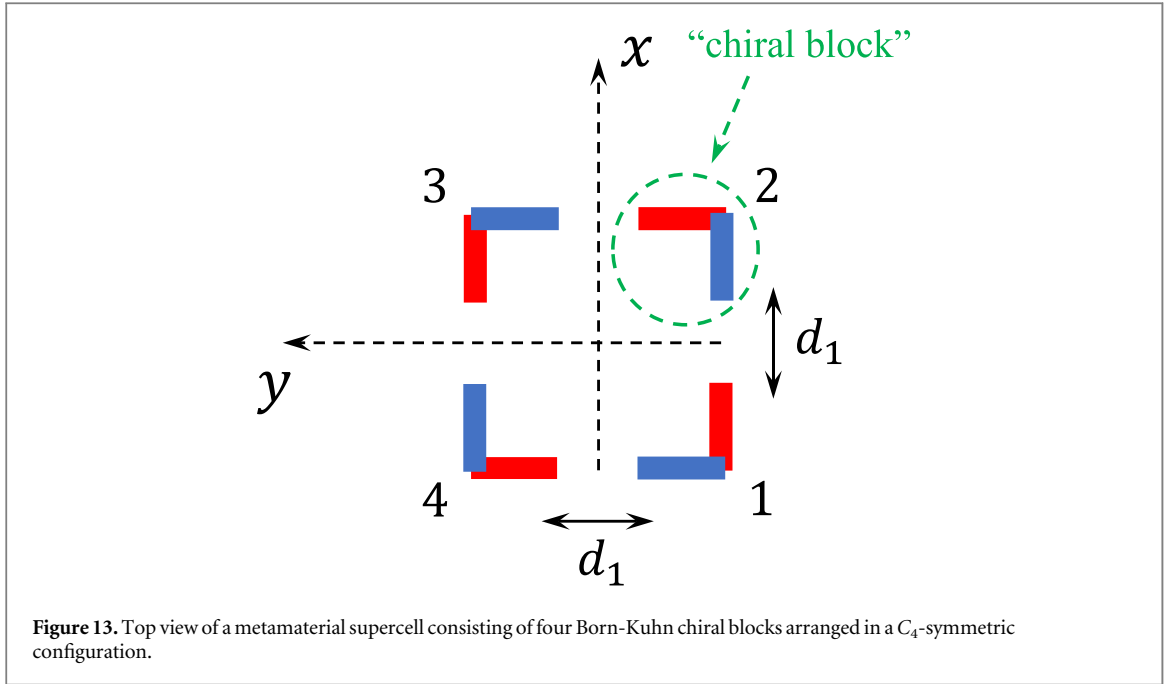
with the solution,

$$x_0 = \frac{q\,\Omega^2}{m(\Omega^4 - \omega_c^4)}\left(\mathcal{E}_x - \frac{\omega_c^2}{\Omega^2}e^{ikd}\mathcal{E}_y\right), \quad y_0 = \frac{q\,\Omega^2}{m(\Omega^4 - \omega_c^4)}\left(\mathcal{E}_y - \frac{\omega_c^2}{\Omega^2}e^{-ikd}\mathcal{E}_x\right). \tag{46}$$

The net field at the observation point is the sum of the incoming field and the field of all radiating charges, *viewed as two planes of pairwise coupled BK oscillators*, which gives, using our generalization of Feynman's formula (26),

$$E_x(z, t) = \left\{\mathcal{E}_x + \frac{i\omega d}{2c}\frac{\omega_p^2\Omega^2}{\Omega^4 - \omega_c^4}\left(\mathcal{E}_x - \frac{\omega_c^2}{\Omega^2}e^{ikd}\mathcal{E}_y\right)\mathcal{A}(z)\right\}e^{-i\omega(t-z/c)}, \tag{47}$$

Figure 13. Top view of a metamaterial supercell consisting of four Born-Kuhn chiral blocks arranged in a C_4-symmetric configuration.

$$E_y(z, t) = \left\{ \mathcal{E}_y + i \frac{\omega d}{2c} \frac{\omega_p^2 \Omega^2}{\Omega^4 - \omega_c^4} \left(\mathcal{E}_y - \frac{\omega_c^2}{\Omega^2} e^{-ikd} \mathcal{E}_x \right) \mathcal{A}(z - d) \right\} e^{-i\omega(t - z/c)}, \qquad (48)$$

where $\mathcal{A} = 1$ for a wide and $\mathcal{A}(z) = 1 - e^{i\pi b^2/(\lambda z)}$ for a narrow beam, respectively, with the plasma frequency now defined by (*cf.* (37)),

$$\omega_p^2 \equiv \frac{\eta q^2}{\varepsilon_0 md}. \qquad (49)$$

In actual experiments, a BK chiral block is made of two identical corner-stacked 'vertically' displaced plasmonic nanorods that are coupled either capacitively or conductively through their mutual near-field interaction [31] (for an earlier theoretical proposal involving inductive coupling see [41]). In addition, in order to avoid anisotropy effects that lead to polarization conversion, the nanorods are arranged in C_4-symmetric configurations (with four nanorod pairs at a time), forming square-shaped 'supercells' out of which metamaterial plates are constructed (figure 13; for details see [31]).

The corresponding equations of motion for pairs 1 and 2 are then (notice the physically motivated minus signs in front of some of the coupling terms),

$$\ddot{x}_1 + \gamma \dot{x}_1 + \omega_0^2 x_1 + \omega_c^2 y_1 = (q/m)\mathcal{E}_x e^{-i\omega t}, \qquad (50)$$

$$\ddot{y}_1 + \gamma \dot{y}_1 + \omega_0^2 y_1 + \omega_c^2 x_1 = (q/m)\mathcal{E}_y e^{-i(\omega t - kd)}, \qquad (51)$$

$$\ddot{x}_2 + \gamma \dot{x}_2 + \omega_0^2 x_2 - \omega_c^2 y_2 = (q/m)\mathcal{E}_x e^{-i(\omega t - kd)}, \qquad (52)$$

$$\ddot{y}_2 + \gamma \dot{y}_2 + \omega_0^2 y_2 - \omega_c^2 x_2 = (q/m)\mathcal{E}_y e^{-i\omega t}, \qquad (53)$$

with the solution,

$$x_{01} = \frac{q}{m} \frac{\Omega^2}{(\Omega^4 - \omega_c^4)} \left(\mathcal{E}_x - \frac{\omega_c^2}{\Omega^2} e^{ikd} \mathcal{E}_y \right), \quad y_{01} = \frac{q}{m} \frac{\Omega^2}{(\Omega^4 - \omega_c^4)} \left(\mathcal{E}_y - \frac{\omega_c^2}{\Omega^2} e^{-ikd} \mathcal{E}_x \right), \qquad (54)$$

$$x_{02} = \frac{q}{m} \frac{\Omega^2}{(\Omega^4 - \omega_c^4)} \left(\mathcal{E}_x + \frac{\omega_c^2}{\Omega^2} e^{-ikd} \mathcal{E}_y \right), \quad y_{02} = \frac{q}{m} \frac{\Omega^2}{(\Omega^4 - \omega_c^4)} \left(\mathcal{E}_y + \frac{\omega_c^2}{\Omega^2} e^{ikd} \mathcal{E}_x \right), \qquad (55)$$

and similarly for pairs 3 and 4. Taking into account that $d \ll z$, so that $\mathcal{A}(z - d) \approx \mathcal{A}(z)$, we get the total transmitted field,

$$E_x(z, t) = \left\{ \left(1 + i \frac{\omega d}{2c} \frac{4\omega_p^2 \Omega^2}{\Omega^4 - \omega_c^4} \mathcal{A}(z) \right) \mathcal{E}_x + \frac{\omega d}{2c} \frac{4\omega_p^2 \omega_c^2}{\Omega^4 - \omega_c^4} \sin(kd) \mathcal{A}(z) \mathcal{E}_y \right\} e^{-i\omega(t - z/c)}, \qquad (56)$$

$$E_y(z,\,t) = \left\{\left(1 + i\,\frac{\omega d}{2c}\,\frac{4\omega_\mathrm{p}^2\Omega^2}{\Omega^4 - \omega_\mathrm{c}^4}\,\mathcal{A}(z)\right)\mathcal{E}_y - \frac{\omega d}{2c}\,\frac{4\omega_\mathrm{p}^2\omega_\mathrm{c}^2}{\Omega^4 - \omega_\mathrm{c}^4}\,\sin(kd)\,\mathcal{A}(z)\,\mathcal{E}_x\right\}e^{-i\omega(t - z/c)}. \qquad (57)$$

Because the BK model ignores any coupling between different chiral blocks, to make it physically reasonable we have to assume that the separation distance d between nanorods in a given BK pair is much smaller than the distance d_1 between nearest such pairs (figure 13). Therefore, in the context of Feynman's approach, the distance d_1 should be viewed as the effective size of individual dipoles that appear in the derivation of his formula. Since that derivation was performed under the assumption of point dipoles, we have to assume that $d_1 \ll \lambda$ and, thus, $d \ll \lambda$, or $kd \ll 1$. Correspondingly, from the point of view of a single chiral block, we are in the long-wavelength (or, quasi-static) limit, in which case we may set

$$\sin(kd) \approx kd, \qquad (58)$$

and get,

$$E_x(z,\,t) = \left\{\left(1 + i\,\frac{\omega\tilde{\chi}d}{2c}\,\mathcal{A}(z)\right)\mathcal{E}_x + \frac{\omega^2\Gamma d}{2c^2}\,\mathcal{A}(z)\,\mathcal{E}_y\right\}e^{-i\omega(t - z/c)}, \qquad (59)$$

$$E_y(z,\,t) = \left\{-\frac{\omega^2\Gamma d}{2c^2}\,\mathcal{A}(z)\,\mathcal{E}_x + \left(1 + i\,\frac{\omega\tilde{\chi}d}{2c}\,\mathcal{A}(z)\right)\mathcal{E}_y\right\}e^{-i\omega(t - z/c)}, \qquad (60)$$

where we formally introduced susceptibility and the nonlocality (or, gyration) parameter,

$$\tilde{\chi} \equiv \frac{4\omega_\mathrm{p}^2\Omega^2}{\Omega^4 - \omega_\mathrm{c}^4}, \qquad \Gamma \equiv \frac{4\omega_\mathrm{p}^2\omega_\mathrm{c}^2 d}{\Omega^4 - \omega_\mathrm{c}^4}, \qquad (61)$$

to make connection with their counterparts in the Born-Kuhn model [31, 39] (the factors of 4 are due to the number of chiral blocks in the supercell). Additionally, if the two BK planes of coupled nanorods are separated by a *transparent* dielectric layer (of thickness $d \ll \lambda$) then, following Feynman's ideology, we may treat such a layer as another plane of oscillating charges with effective susceptibility $\chi_\mathrm{dielectric}$ and get (our main result),

$$E_x(z,\,t) = \left\{\left(1 + i\,\frac{\omega\chi d}{2c}\,\mathcal{A}(z)\right)\mathcal{E}_x + \frac{\omega^2\Gamma d}{2c^2}\,\mathcal{A}(z)\,\mathcal{E}_y\right\}e^{-i\omega(t - z/c)}, \qquad (62)$$

$$E_y(z,\,t) = \left\{-\frac{\omega^2\Gamma d}{2c^2}\,\mathcal{A}(z)\,\mathcal{E}_x + \left(1 + i\,\frac{\omega\chi d}{2c}\,\mathcal{A}(z)\right)\mathcal{E}_y\right\}e^{-i\omega(t - z/c)}, \qquad (63)$$

where

$$\chi = \tilde{\chi} + \chi_\mathrm{dielectric}. \qquad (64)$$

Diagonalization of the system (62), (63) immediately gives the two eigenmodes (the left (LCP) and the right (RCP) circularly polarized electromagnetic waves) and their respective eigenvalues, $\mathcal{T}_\mathrm{L,R}$,

$$\begin{pmatrix}\mathcal{E}_x \\ \mathcal{E}_y\end{pmatrix}_\mathrm{L,R} = \frac{\mathcal{E}_0}{\sqrt{2}}\begin{pmatrix}1 \\ \pm i\end{pmatrix}, \qquad \mathcal{T}_\mathrm{L,R}(z) = 1 + i\,\frac{\omega d}{2c}\left(\chi \pm \frac{\omega\Gamma}{c}\right)\mathcal{A}(z), \qquad (65)$$

where $\mathcal{E}_0$ is the amplitude of the incoming wave. When these modes pass through a BK plate, their polarization stays the same, while the amplitude is multiplied by the corresponding eigenvalue (*cf.* Equation (36)), which therefore determines the transmitted intensity (as a function of the distance), $|\mathcal{T}_\mathrm{L,R}(z)|^2$.

Introducing two 'brightness' amplitudes,

$$\mathcal{B}_\mathrm{L,R}(z) = i\,\frac{\omega d}{2c}\left(\chi \pm \frac{\omega\Gamma}{c}\right)\mathcal{A}(z), \qquad (66)$$
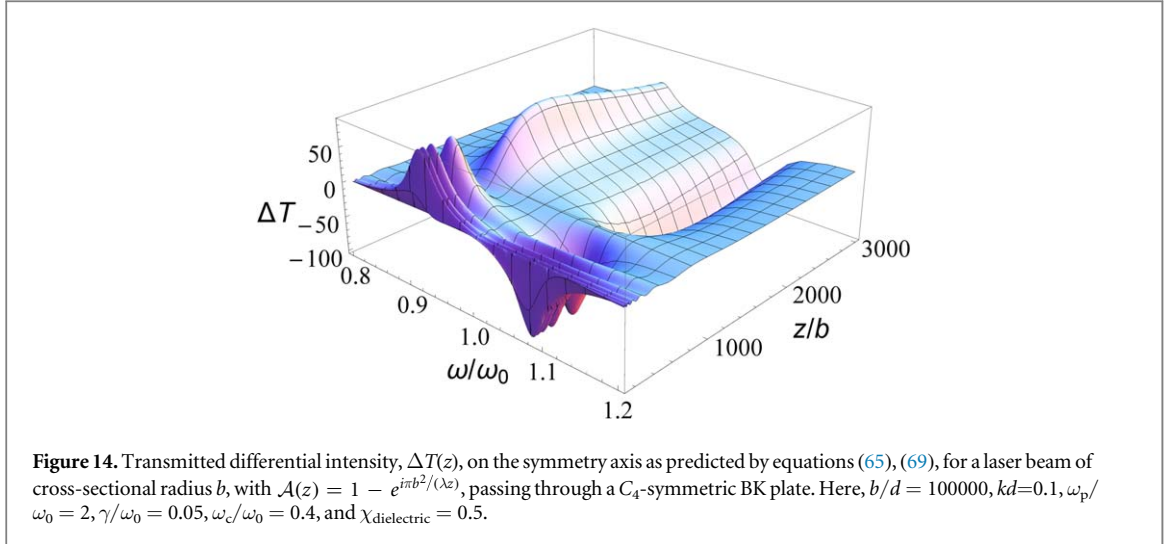
which characterize contributions to the respective transmitted modes due to the radiating (portion of the) BK plate, we can define two additional experimentally relevant quantities: differential brightness (which generalizes to narrow beams the concept of optical rotatory dispersion (ORD), *cf.* Equation (S20.2) in [30]),

$$\mathrm{ORD} \sim \Delta B(z) \equiv |\mathcal{B}_\mathrm{L}(z)|^2 - |\mathcal{B}_\mathrm{R}(z)|^2 = \frac{\omega^2 d^2}{c^2}\,\frac{\omega}{c}(\chi'\Gamma' + \chi''\Gamma'')|\mathcal{A}(z)|^2, \qquad (67)$$

and differential absorbance (which generalizes the concept of circular dichroism (CD), *cf.* Equation (7) in [31]),

$$\mathrm{CD} \sim \Delta A(z) \equiv -\frac{\omega d}{c}\,\frac{2\omega}{c}(\Gamma''\,\mathcal{A}'(z) + \Gamma'\,\mathcal{A}''(z)), \qquad (68)$$

where we used primes to indicate the real and imaginary parts of various quantities involved, $\chi = \chi' + i\chi''$, $\Gamma = \Gamma' + i\Gamma''$, $\mathcal{A} = \mathcal{A}' + i\mathcal{A}''$. It is then straightforward to show using simple algebra that (unnormalized) transmitted differential intensity is given by

Figure 14. Transmitted differential intensity, $\Delta T(z)$, on the symmetry axis as predicted by equations (65), (69), for a laser beam of cross-sectional radius b, with $\mathcal{A}(z) = 1 - e^{i\pi b^2/(\lambda z)}$, passing through a C_4-symmetric BK plate. Here, $b/d = 100000$, kd=0.1, $\omega_{\mathrm{p}}/\omega_0 = 2$, $\gamma/\omega_0 = 0.05$, $\omega_{\mathrm{c}}/\omega_0 = 0.4$, and $\chi_{\mathrm{dielectric}} = 0.5$.

$$\Delta T(z) \equiv |\mathcal{T}_{\mathrm{L}}(z)|^2 - |\mathcal{T}_{\mathrm{R}}(z)|^2 = \Delta B(z) + \Delta A(z), \tag{69}$$

which is plotted for a laser beam of finite width in figure 14. For a wide beam ($\mathcal{A} = 1$) this becomes z-independent,

$$\Delta T = \frac{4\,\omega_{\mathrm{p}}^2\,\omega_{\mathrm{c}}^2\,(\omega^2 d^2/c^2)\{4(\omega_0^2 - \omega^2)(\omega_{\mathrm{p}}^2\,(\omega d/c) - \gamma\omega) + \chi_{\mathrm{dielectric}}\,(\omega d/c)((\omega_0^2 - \omega^2)^2 - \gamma^2\omega^2 - \omega_{\mathrm{c}}^4)\}}{((\omega^2 - \omega_0^2)^2 - \omega_{\mathrm{c}}^4)^2 + 2\,\gamma^2\omega^2((\omega^2 - \omega_0^2)^2 + \omega_{\mathrm{c}}^4) + \gamma^4\omega^4}, \tag{70}$$

as shown in figure 15. Notice that for sufficiently small values of kd, when damping becomes dominant, the numerator in (70) may become negative and we get *abnormal* behavior of ΔT (though the effect is expected to be quite weak), as shown in figures 16 and 17.

Finally, for an incoming beam *linearly* polarized along the x-axis, with $\mathcal{E}_x = \mathcal{E}_0$, $\mathcal{E}_y = 0$, the corresponding transmitted field is elliptically polarized and is given by

$$E_x(z,\,t) = \left(1 + i\,\frac{\omega\chi d}{2c}\,\mathcal{A}(z)\right)\mathcal{E}_0\,e^{-i\omega(t - z/c)}, \quad E_y(z,\,t) = -\frac{\omega^2\Gamma d}{2c^2}\,\mathcal{A}(z)\,\mathcal{E}_0\,e^{-i\omega(t - z/c)}. \tag{71}$$

If we work with a wide beam ($b = \infty$, $\mathcal{A} = 1$), assume no losses ($\gamma = 0$), and take ω to be far from each of the two resonances, $\omega_{\pm} = \sqrt{\omega_0^2 \pm \omega_{\mathrm{c}}^2}$, then the χ-dependent term can be dropped (with elliptical polarization degenerating into linear), and we get the standard expression for polarization rotation angle,
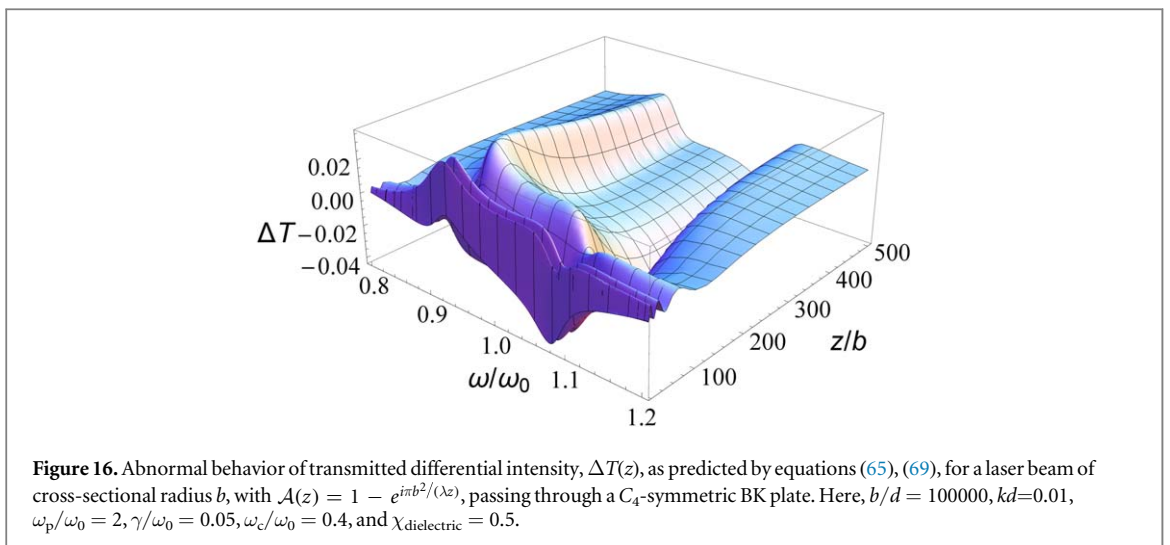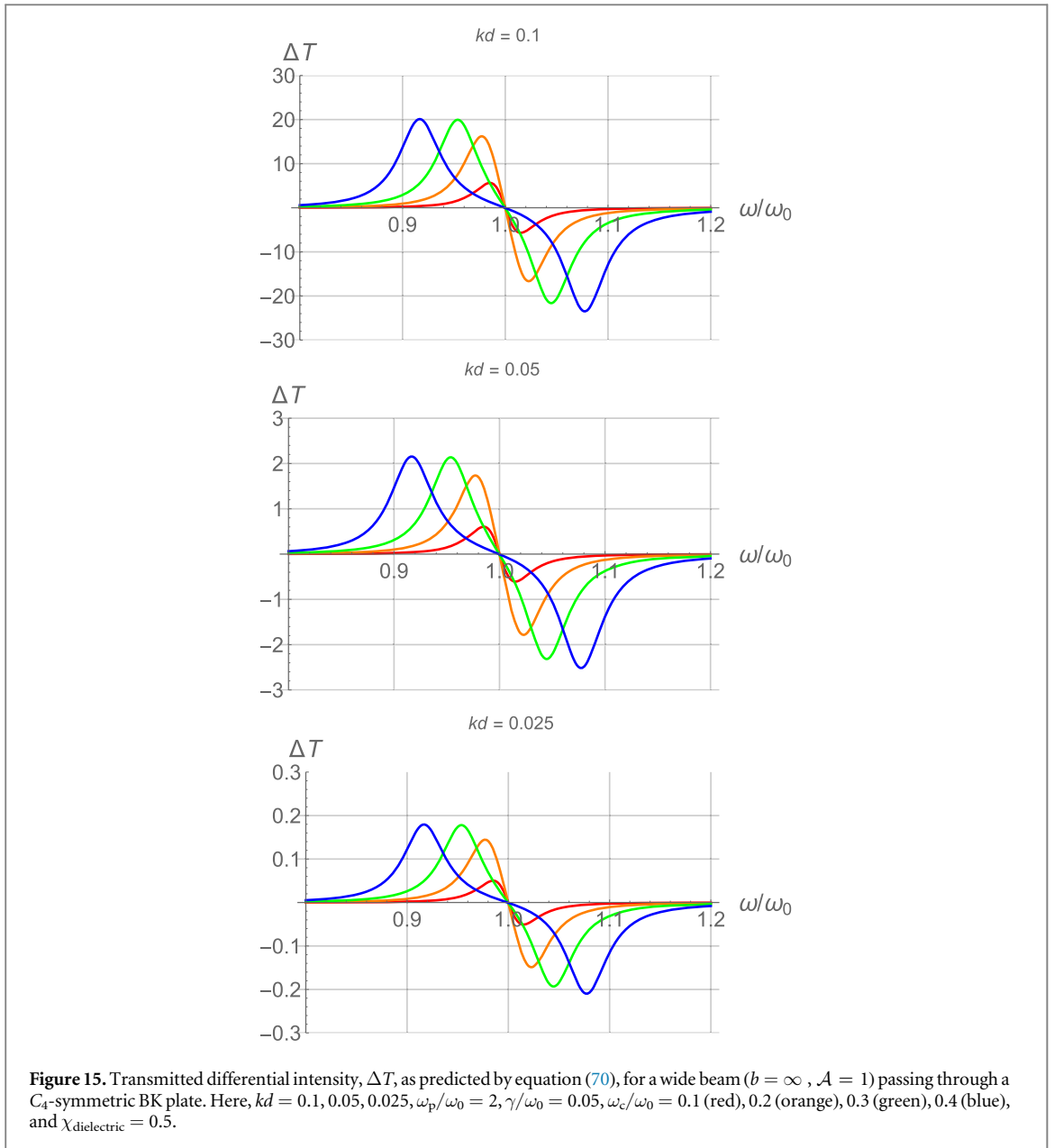
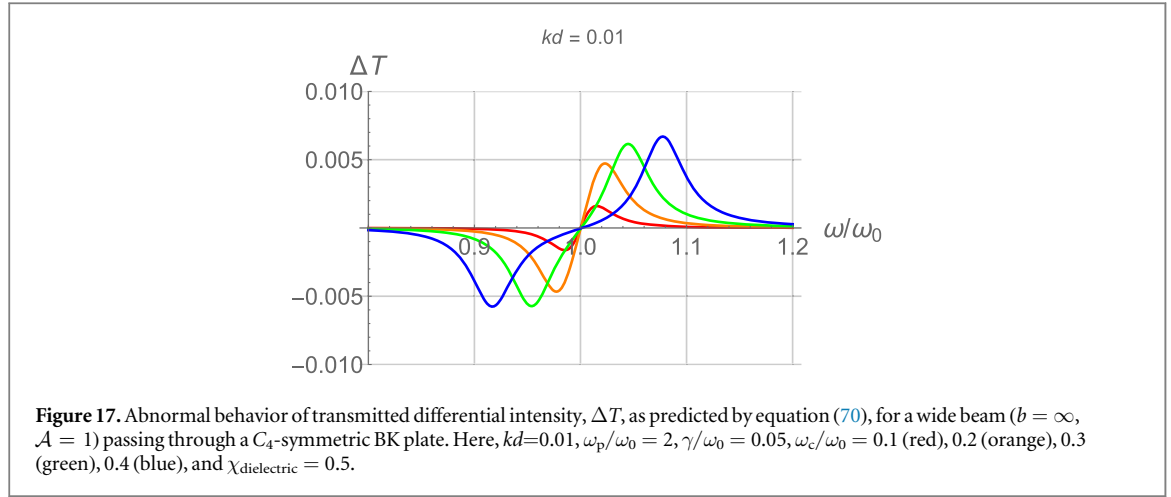$$\psi \approx -\frac{\omega^2}{2c^2}\,\Gamma d, \tag{72}$$

where the minus sign is due to our left-handed choice for the chirality of the BK plate. Supplemental Movies 1, 2, and 3 show how, in accordance with our theory, linearly polarized electromagnetic waves of different frequencies change their polarization upon passing through a chiral plate located at the origin. (The incident and transmitted amplitudes in Movies 2 and 3 have been re-scaled differently to enhance visualization.)

4. Summary

We developed a simple physically motivated theoretical method for the analysis of electromagnetic processes in nanorod-based plasmonic metamaterials that is not rooted in macroscopic electrodynamics. Specific predictions were made for a single sheet of aligned nanorods and for a chiral plate made of corner-stacked nanorods, which can easily be extended to more complicated multi-stacked structures consisting of dipole-like basic elements. We proposed several interference experiments to test our theory that can be performed using readily available equipment. Due to high sensitivity of the predicted interference patterns to small changes in various system's parameters (such as, e. g., surface density of the deposited nanorods or resonant frequencies of individual nanorods) the proposed experimental implementations could potentially be used in the development of quality standards for various metamaterial devices. In principle, our approach should also be able to handle systems that exhibit nonlinear and higher-order multipole behavior, though the mathematical details accompanying such generalization may likely become rather complicated.

Figure 15. Transmitted differential intensity, ΔT, as predicted by equation (70), for a wide beam ($b = \infty$, $\mathcal{A} = 1$) passing through a C_4-symmetric BK plate. Here, $kd = 0.1, 0.05, 0.025$, $\omega_{\mathrm{p}}/\omega_0 = 2$, $\gamma/\omega_0 = 0.05$, $\omega_{\mathrm{c}}/\omega_0 = 0.1$ (red), 0.2 (orange), 0.3 (green), 0.4 (blue), and $\chi_{\mathrm{dielectric}} = 0.5$.

Figure 16. Abnormal behavior of transmitted differential intensity, $\Delta T(z)$, as predicted by equations (65), (69), for a laser beam of cross-sectional radius b, with $\mathcal{A}(z) = 1 - e^{i\pi b^2/(\lambda z)}$, passing through a C_4-symmetric BK plate. Here, $b/d = 100000$, $kd=0.01$, $\omega_{\mathrm{p}}/\omega_0 = 2$, $\gamma/\omega_0 = 0.05$, $\omega_{\mathrm{c}}/\omega_0 = 0.4$, and $\chi_{\mathrm{dielectric}} = 0.5$.

Figure 17. Abnormal behavior of transmitted differential intensity, ΔT, as predicted by equation (70), for a wide beam ($b = \infty$, $\mathcal{A} = 1$) passing through a C_4-symmetric BK plate. Here, kd=0.01, $\omega_p/\omega_0 = 2$, $\gamma/\omega_0 = 0.05$, $\omega_c/\omega_0 = 0.1$ (red), 0.2 (orange), 0.3 (green), 0.4 (blue), and $\chi_{\text{dielectric}} = 0.5$.

Data availability statement

All data that support the findings of this study are included within the article (and any supplementary files).

Appendix A. Elementary theory of scattering on a plane of charges

Here for the sake of completeness we re-derive equations (36) and (47), (48) in the case of a wide beam ($b = \infty$, $\mathcal{A} = 1$) using a more traditional approach to scattering. Our discussion parallels that of [42].

For harmonically oscillating fields, E, B, charges, ρ, and currents, j, Maxwell's equations take the form (Coulomb's constant dropped, the magnetic field B is re-scaled by the speed of light c),

$$\nabla \cdot \boldsymbol{E}(\boldsymbol{r}, \omega) = 4\pi\rho(\boldsymbol{r}, \omega), \tag{A1}$$

$$\nabla \times \boldsymbol{E}(\boldsymbol{r}, \omega) = \frac{i\omega}{c}\boldsymbol{B}(\boldsymbol{r}, \omega), \tag{A2}$$

$$\nabla \cdot \boldsymbol{B}(\boldsymbol{r}, \omega) = 0, \tag{A3}$$

$$\nabla \times \boldsymbol{B}(\boldsymbol{r}, \omega) = -\frac{i\omega}{c}\boldsymbol{E}(\boldsymbol{r}, \omega) + \frac{4\pi}{c}\boldsymbol{j}(\boldsymbol{r}, \omega). \tag{A4}$$

If we assume a scenario in which a plane electromagnetic wave propagating in the positive z-direction strikes at normal incidence infinitesimally thin (essentially, δ-function like) slab of some material located at $z = 0$, then for points outside of the xy-plane the solution is

$$\boldsymbol{E}(z < 0, \omega) = \begin{pmatrix} \mathcal{E}_x^{(i)} \\ \mathcal{E}_y^{(i)} \\ 0 \end{pmatrix} e^{-i(\omega t - kz)} + \begin{pmatrix} \mathcal{E}_x^{(r)} \\ \mathcal{E}_y^{(r)} \\ 0 \end{pmatrix} e^{-i(\omega t + kz)}, \quad \boldsymbol{E}(z > 0, \omega) = \begin{pmatrix} \mathcal{E}_x^{(t)} \\ \mathcal{E}_y^{(t)} \\ 0 \end{pmatrix} e^{-i(\omega t - kz)}, \tag{A5}$$

and similarly for the magnetic field, with

$$\mathcal{B}_x^{(i)} = -\mathcal{E}_y^{(i)}, \quad \mathcal{B}_y^{(i)} = \mathcal{E}_x^{(i)}, \tag{A6}$$

$$\mathcal{B}_x^{(r)} = \mathcal{E}_y^{(r)}, \quad \mathcal{B}_y^{(r)} = -\mathcal{E}_x^{(r)}, \tag{A7}$$

$$\mathcal{B}_x^{(t)} = -\mathcal{E}_y^{(t)}, \quad \mathcal{B}_y^{(t)} = \mathcal{E}_x^{(t)}, \tag{A8}$$

and the boundary conditions at the interface,

$$\mathcal{E}_x^{(i)} + \mathcal{E}_x^{(r)} = \mathcal{E}_x^{(t)}, \quad \mathcal{E}_y^{(i)} + \mathcal{E}_y^{(r)} = \mathcal{E}_y^{(t)}, \tag{A9}$$

$$\mathcal{B}_x^{(t)} - (\mathcal{B}_x^{(i)} + \mathcal{B}_x^{(r)}) = \frac{4\pi}{c}\mathcal{K}_y, \quad \mathcal{B}_y^{(t)} - (\mathcal{B}_y^{(i)} + \mathcal{B}_y^{(r)}) = -\frac{4\pi}{c}\mathcal{K}_x, \tag{A10}$$

where $\mathcal{E}^{(i,r,t)}$ and $\mathcal{B}^{(i,r,t)}$ are the incident, reflected, and transmitted amplitudes, respectively, and $(\mathcal{K}_x, \mathcal{K}_y)$ is the bound surface current density. Combining all these relations gives the boundary conditions in terms of the electric field only,

$$\mathcal{E}_x^{(i)} - \mathcal{E}_x^{(r)} - \mathcal{E}_x^{(t)} = \frac{4\pi}{c}\mathcal{K}_x, \quad \mathcal{E}_y^{(i)} - \mathcal{E}_y^{(r)} - \mathcal{E}_y^{(t)} = \frac{4\pi}{c}\mathcal{K}_y, \tag{A11}$$

which for transmitted amplitudes become

$$\mathcal{E}_x^{(t)} = \mathcal{E}_x^{(i)} - \frac{2\pi}{c}\mathcal{K}_x, \quad \mathcal{E}_y^{(t)} = \mathcal{E}_y^{(i)} - \frac{2\pi}{c}\mathcal{K}_y. \tag{A12}$$

For a single sheet of aligned nanorods, we get on the basis of equation (35),

$$\dot{x}(t) = -i\omega x_0 e^{-i\omega t}, \quad x_0 = \frac{q}{m\Omega^2}\mathcal{E}_x^{(i)}, \quad \dot{y}(t) = 0, \tag{A13}$$

and

$$\mathcal{K}_x = \eta q \dot{x}(t) = -i\omega \frac{\eta q^2}{mD}\frac{D}{\Omega^2}\mathcal{E}_x^{(i)}, \quad \mathcal{K}_y = 0, \tag{A14}$$

which upon restoring Coulomb's constant recovers equation (36) with $\mathcal{A} = 1$ (wide beam). Notice that in our derivation we assumed that the nanorods were not densely packed and were driven by the *local* field, which, following standard practice [39, 40], we took to be $\mathcal{E}_x^{(i)}$. This is in contrast with the tightly packed scenario which would typically be handled using macroscopic electrodynamics by taking

$$\mathcal{K}_x = \sigma_x \mathcal{E}_x^{(t)}, \tag{A15}$$

where σ_x is the conductivity, with the result (see equation (1) in [43]),

$$\mathcal{E}_x^{(t)} = \frac{\mathcal{E}_x^{(i)}}{1 + 2\pi\sigma_x/c}. \tag{A16}$$

The tightly packed scenario clearly allows the possibility of zero transmission for very large σ_x (think of aluminum foil reflecting all incident light, for example). In our theory that situation would roughly correspond to

$$\dot{x}(t) = -i\omega x_0 e^{-i\omega t}, \quad x_0 = \frac{q}{m\Omega^2}\mathcal{E}_x^{(t)}, \quad \dot{y}(t) = 0, \tag{A17}$$

[compare with equation (A13) above], which after restoring Coulomb's constant would give,

$$\mathcal{T}(z) \equiv \frac{\mathcal{E}_x^{(t)}}{\mathcal{E}_x^{(i)}} = \frac{1}{1 - i\frac{\omega D}{2c}\frac{\omega_{p1}^2}{\Omega^2}}, \tag{A18}$$

and, in first order,

$$\mathcal{T}(z) \approx 1 + i\frac{\omega D}{2c}\frac{\omega_{p1}^2}{\Omega^2}, \tag{A19}$$

in agreement with equation (36).

For a chiral plate viewed as two planes of orthogonally oscillating charges, the first set of boundary conditions is

$$\mathcal{E}_x^{(t)} = \mathcal{E}_x^{(i)} - \frac{2\pi}{c}\mathcal{K}_x, \quad \mathcal{E}_y^{(t)} = \mathcal{E}_y^{(i)}, \tag{A20}$$

while the second is shifted in phase,

$$\mathcal{E}_x^{(t)}e^{ikd} = \mathcal{E}_x^{(i)}e^{ikd}, \quad \mathcal{E}_y^{(t)}e^{ikd} = \mathcal{E}_y^{(i)}e^{ikd} - \frac{2\pi}{c}\mathcal{K}_y, \tag{A21}$$

which on the basis of (44) and (46) give

$$\mathcal{K}_x = -i\omega\frac{\eta q^2}{md}\frac{\Omega^2 d}{\Omega^4 - \omega_c^4}\left(\mathcal{E}_x^{(i)} - \frac{\omega_c^2}{\Omega^2}e^{ikd}\mathcal{E}_y^{(i)}\right), \quad \mathcal{K}_y = -i\omega\frac{\eta q^2}{md}\frac{\Omega^2 d}{\Omega^4 - \omega_c^4}\left(\mathcal{E}_y^{(i)} - \frac{\omega_c^2}{\Omega^2}e^{-ikd}\mathcal{E}_x^{(i)}\right)e^{ikd}, \tag{A22}$$

recovering equations (47) and (48) in the case of a wide beam.

ORCID iDs

Andrei Galiautdinov https://orcid.org/0000-0001-5752-9296

References

[1] Maxwell J C 1873 *A Treatise on Electricity and Magnetism* (Oxford: Clarendon)
[2] Lorentz H A 1892 *La théorie électromagnétique de Maxwell et son application aux corps mouvants* (Leiden: E.J. Brill)
[3] Lorentz H A 1906 *Versuch einer Theorie der electrischen und optischen Erscheinungen in bewegten Körpern* (Leipzig: B.G. Teubner)
[4] Landau L, Lifshitz E and Pitaevskii L 1984 *Electrodynamics of Continuous Media* (Oxford: Butterworth-Heinenann)

[5] Jackson J D 1999 *Classical Electrodynamics* (New York: Wiley)

[6] Mikhailov S A 2019 *APL Photonics* **4** 034501

[7] Zangwill A 2013 *Modern Electrodynamics* (Cambridge: Cambridge University Press)

[8] Dirac P A M 1981 *The Principles of Quantum Mechanics* (Oxford: Oxford University Press)

[9] Stodolna A S, Rouzée A, Lépine F, Cohen S, Robicheaux F, Gijsbertsen A, Jungmann J, Bordas C and Vrakking M 2013 *Phys. Rev. Lett.* **110** 213001

[10] Smith D, Vier D, Koschny T and Soukoulis C 2005 *Phys. Rev. E* **71** 036617

[11] Kwon D-H, Werner D H, Kildishev A V and Shalaev V M 2008 *Opt. Express* **16** 11822

[12] Wang B, Zhou J, Koschny T, Kafesaki M and Soukoulis C M 2009 *J. Opt. A: Pure Appl. Opt.* **11** 114003

[13] Cai W and Shalaev V M 2010 *Optical Metamaterials* (New York: Springer)

[14] Tassin P, Koschny T and Soukoulis C M 2012 *Physica B* **407** 4062

[15] Sihvola A H and Lindell I V 1991 *Microwave Opt. Technol. Lett.* **4** 295

[16] Lindell I, Sihvola A, Tretyakov S and Viitanen A J 1994 *Electromagnetic Waves in Chiral and Bi-isotropic Media* (Boston: Artech House)

[17] Vinogradov A P 2002 *Phys. Usp.* **45** 331

[18] Maier S A 2007 *Plasmonics: Fundamentals and Applications* (Berlin: Springer)

[19] Schäferling M, Dregely D, Hentschel M and Giessen H 2012 *Physical Review X* **2** 031010

[20] Yao K and Liu Y 2014 *Nanotechnology Reviews* **3** 177

[21] Goerlitzer E S, Puri A S, Moses J J, Poulikakos L V and Vogel N 2021 *Adv. Opt. Mater.* **9** 2100378

[22] Lagarkov A and Sarychev A 1996 *Physical Review B* **53** 6318

[23] Ivanov A, Shalygin A, Lebedev V, Vorobev P, Vergiles S and Sarychev A 2012 *Appl. Phys. A* **107** 17

[24] Vinogradov A P 2001 *Electrodynamics of Composites* (Moscow: URSS)

[25] Vinogradov A and Merzlikin A 2002 *Advances in Electromagnetics of Complex Media and Metamaterials* (Dordrecht: Springer) 341–61

[26] Sarychev A K and Shalaev V M 2007 *Electrodynamics of Metamaterials* (Singapore: World Scientific)

[27] Klimov V 2014 *Nanoplasmonics* (Boca Raton, FL: CRC Press)

[28] Feynman R P, Leighton R B and Sands M 2006 *The Feynman Lectures on Physics: The Definitive Edition* (Reading, MA: Addison-Wesley) Volume I

[29] Lebedev N N 1972 *Special Functions and Their Applications* (New York: Dover Publications)

[30] Davis M S, Zhu W, Lee J K, Lezec H J and Agrawal A 2019 *Science Advances* **5** eaav8262

[31] Yin X, Schäferling M, Metzger B and Giessen H 2013 *Nano Lett.* **13** 6238

[32] Yin X, Schäferling M, Michel A-K U, Tittl A, Wuttig M, Taubner T and Giessen H 2015 *Nano Lett.* **15** 4255

[33] Vestler D *et al* 2018 *Opt. Express* **26** 17841

[34] Zheng J, Cheng X, Zhang H, Bai X, Ai R, Shao L and Wang J 2021 *Chem. Rev.* **121** 13342

[35] Kumar V, Rossi A W, Lawson Z R, Neal R D, Hachtel J A, Neretina S, Maseillo D J and Camden J P 2023 *Microsc. Microanal.* **29** 641

[36] Luo X, Wang X, Zhang L, Song L, Sun Z, Zhao Y, Su F and Huang Y 2023 *Nano Res.* **16** 5087

[37] Kuhn W 1930 *Trans. Faraday Soc.* **26** 293

[38] Born M 1935 *Proceedings of the Royal Society of London. Series A - Mathematical and Physical Sciences* **150** 84

[39] Svirko Y P and Zheludev N I 2000 *Polarization of Light in Nonlinear Optics* (Chichester, UK: Wiley)

[40] Schäferling M 2017 *Chiral Nanophotonics* (Cham: Springer)

[41] Svirko Y, Zheludev N and Osipov M 2001 *Appl. Phys. Lett.* **78** 498

[42] Chiu K, Lee T and Quinn J 1976 *Surf. Sci.* **58** 182

[43] Mikhailov S A 2004 *Physical Review B* **70** 165311